Liquid film thickness behaviour within a large diameter vertical 180º return bend

M. Abdulkadir[1, 2, 3], A. Azzi[4], D. Zhao[5], I.S. Lowndes[1] and B.J. Azzopardi[1]

[1]Process and Environmental Engineering Research Division, Faculty of Engineering, University of Nottingham, University Park, Nottingham, NG7 2RD, United Kingdom

[2] Department of Chemical Engineering, Federal University of Technology, Minna, Niger State, Nigeria

[3]Department of Petroleum Engineering, African University of Science and Technology, Abuja, Nigeria

[4]Université des Sciences et de la Technologie Houari Boumediene (USTHB), FGMGP, LTPMP, Bab Ezzouar, 16111, Algiers, Algeria

[5]Department of Applied Science, London South Bank University, 103 Borough Road, London, SE1 0AA, United Kingdom

*Corresponding author: mukhau@futminna.edu.ng

Abstract: Experimental results of liquid film thickness distribution of an air–water mixture flowing through a vertical 180° return bend are reported. Measurements of liquid film thickness were achieved using flush mounted pin and parallel wire probes. The bend has a diameter of 127 mm and a curvature ratio (*R/D*) of 3. The superficial velocities of air ranged from 3.5 to 16.1 m/s and those for water from 0.02 to 0.2 m/s. At these superficial velocity ranges, the flow pattern investigated in this work focused on churn and annular flows. It was found that at liquid and gas superficial velocities of 0.02 m/s and 6.2 m/s, respectively, the averaged liquid film thickness peak at 90º. At gas superficial velocity of 16.1 m/s, the relationship between them is linear due to the shear forces overcoming gravity. Additionally, it was found that deposition of entrained droplets keeps the liquid film on the outside of the bend. The results of polar plots of average liquid film thickness in the bend showed that the distribution of the liquid film is not symmetrical with thicker films on the inside of the bend due to the action of gravity. Experimental results on average liquid film thickness showed good agreement with the simulation data reported in the literature.

Keywords: churn and annular flows, liquid film thickness, 180° bend, large diameter, pin probes, wire probes.

1. Introduction

Two-phase gas–liquid flow in bends is widely encountered in industrial equipment ranging from steam generators in nuclear power reactor, fired reboilers in oil refining and hydrocarbon processing plant, fossil fuelled boilers and pipework in oil/gas production, refinery and chemical plants. Though notionally a simple geometry, their use with gas liquid flow is made complex because of the effect of gravity which tends to stratify the phases. This means that several parameters must be quantified to ensure that the correct effect of the bend is realised and understood. The first, and most obvious, parameter is the angle between the inlet and outlet pipes. This tends to come in certain prescribed values such as 90° or 180°. The second parameter is the orientation of the inlet and outlet pipes. Even confining ourselves to 180° bends there are U bends, inverted U bends and C bends. The first two have vertical pipes, the last horizontal pipes. However, for C bends there needs to be a specification of what is the orientation of the plane of the bend relative to gravity, taking into account the direction of flow. The extent of the differences for vertical upwards, 45°, and horizontal versions are illustrated by Sakamoto *et al.* (2004). Here, we focus on inverted U bends for which papers have been written by Golan and Stenning (1969), Hills (1973), Anderson and Hills (1974), Usui *et al.* (1983), Hoang and Davies (1984), Takemura *et al.* (1986). Golan and Stenning (1969) and Takemura *et al.* (1986) who noted that they act as phase separators because of the combined effect of centrifugal forces and gravity. In a U bend the two forces act in the same direction, usually sending the liquid to the outside of the bend and gas to the inside. In the inverted U-bend case the forces can act in opposite directions at lower liquid flow rates. However, at higher liquid flow rates, the centrifugal forces dominate and the liquid goes to the outside of the bend. Takemura *et al.* (1986) confirmed these trends from wall temperature excursions in electrically heated experiments. Golan and Stenning (1969) reported that the effect of the bend on phase distribution disappeared by 10 pipe

diameters downstream of the end of the bend for the inverted U-bend case and 4 pipe diameter for the U-bend. The two major applications of inverted U bends are steam generators (typical pipe diameter ~25 mm) and fired reboilers (typical pipe diameter 100-200 mm). It is noted that the work referred to above employed pipe diameters between 18 and 51 mm. Here, the focus is on the latter equipment. Fired reboilers are designed in two parts, the flame side and the process side. The former uses standard furnace models. The main thrust in the latter is about the selection of tube dimensions using sensible and standard sizes so that the required area is fitted around the flames into a reasonable volume. Tube diameters are chosen to keep process side pressure drops low. There is a recognition that coking, the breaking down of the hydrocarbons to produce a form of carbon, can be a problem which will occur if there are unsaturated hydrocarbons present and the wall temperatures rise above critical values. These higher temperatures are associated with dryout of the film of liquid flowing on the walls of the tubes. The term dryout is often associated with the physical mechanism of the drying out of the liquid phase in the process side of the equipment due to evaporation and entrainment that occurs in the annular flow pattern. Current design practice uses a simple rule of thumb–the process mass flux (mass flow rate per unit cross-section of tube must be greater than 1000 kg/m^{2}s. Observation during plant operation had shown that dryout, as witnessed by coking occurred just before bends. Indeed, the bend and part of the pipe upstream are sometimes lagged to prevent coking. Chong *et al.* (2005) modelled the mainly annular flow which occurs in these systems. They allowed for evaporation of the film, its depletion by entrainment into drops and its augmentation by drop deposition. They also allowed for the effect of the bends by assuming that all drops are deposited as they pass through the bend. Their results showed that dryout usually occurs just before the bend. They also found that there was a boundary on a heat flux versus mass flux plot which identified when dryout would occur. For heat fluxes which are typically employed, the corresponding

mass flux is 1000 kg/m^{2}s confirming the rule of thumb mentioned above. Predictions of the occurrences of dryout are hence vital for the design optimization, in terms of safety, cost and efficiency of industrial equipment.

1.1 Two-phase film thickness distribution in 180^o bends

Alves (1954) studied air–water and air–oil flow in a four pass one inch bore horizontal pipeline contactor. Between each pass there was a return bend in a vertical plane, the direction of flow being upwards. The curvature ratio *R/D* was equal to 14. He observed that annular flow, which occurred in the horizontal passes for a superficial gas Reynolds number greater than 40000, was stable in the bend. Visual observation suggested that the liquid film was thicker on the inside of the bend than on the outside.

Hills (1973) and Anderson and Hills (1974), reported data on liquid film thickness, axial pressure profiles, gas velocity distribution, and droplet entrainment in the annular flow regimes in an inverted 180^o return bend. The diameter and radius of curvature of the bend are 25 and 305 mm, respectively. They reported that an increase in film thickness on the inside of the bend can be attributed to the action of gravity and to the secondary flow existing in the gas phase. They observed a change in flow pattern from annular to stratified flow in the bend at low liquid flow rates. On the other hand, for the high liquid flow rates, a local maximum in the film thickness was seen on the inside and outside of the bend.

The distributions of water films and entrained droplets in air–water annular flows in 180^o horizontal bend were investigated by Balfour and Pearce (1978) using sampling probes. The diameter and radius of curvature of the bend are 25 and 48.5 mm, respectively. They took a

series of measurements with the probes positioned at 45^o intervals around the tube exit and at varying radii. They concluded that in those annular flows where the air speed is high, many of the entrained droplets are thrown very rapidly to the wall and that the entrained fraction tends to be negligible for high quality annular flows where the films are thin.

Usui *et al* (1980, 1981, and 1983) measured the average void fraction over the bend using quick closing valves. Whilst the horizontal and vertical up-flow cases could be reasonably represented by the correlation of Smith (1971) - except at the lowest quality - the down-flow data was significantly under predicted. In the latter case, they proposed a correlation in terms of a modified Froude number, *Fr*. *Fr*, is given by equation (1).

$$Fr = \frac{\rho_L U_{SL}^{\ 2}}{(\rho_L - \rho_G) R_b g (1-\varepsilon_{gs})^2} \left[1 - \frac{\rho_G}{\rho_L} \left\{ \frac{U_{SG}(1-\varepsilon_{gs})}{U_{SL}\varepsilon_{gs}} \right\}^2 \right] \qquad (1)$$

Where, R_b is the radius of the bend, g is the acceleration due to gravity, ε_{gs} the value in the straight pipe, U_{SL} and U_{SG} represent liquid and gas superficial velocities, respectively, and ρ_L and ρ_G represent liquid and gas densities, respectively.

Tingkuan *et al*. (1986) conducted experimental work involving flow pattern transitions over wide velocity ranges during co-current air–water flow in a 21.5 mm internal diameter vertical U-shaped tube with a bend of radii 694, 500 and 320 mm, respectively. They determined the flow patterns using visual observation and electrical conductance probe. They then compared their transition data to those reported by Mandhane *et al*. (1974) and Weisman *et al*. (1981). Mandhane *et al.* (1974) carried out experimental work in a 50 mm internal diameter horizontal pipe using air–water as the model fluid while on the other hand Weisman *et al.* (1981) conducted experimental work in a 12 mm, 25 mm and 51 mm internal diameter

vertical and upwardly inclined pipes using air–water. Tingkuan *et al*. (1986) concluded that their data fitted both the Mandhane *et al*. (1974) and Weisman *et al*. (1981) transition criteria well and that the major effect of the bend on the flow patterns is the considerable expansion of the stratified flow regime. This conclusion confirmed the earlier work of Hills (1973).

Yu *et al* (1989) measured void fraction using a fibre optic probe over cross sections at different angles around the bend. They found that the equations proposed by Usui (1992) over-predict in upward flow and under-predict in downward flow. For the cross-sectionally averaged void fraction they found an initial decrease in up flow followed by an increase. For downward flow, the behaviour was much more complex. As Yu *et al.* (1989) were working in the bubbly and slug flow regions, the observed decrease in void fraction probably corresponds to the observed flow reversal, an occurrence that would increase the liquid holdup.

Poulson (1991) studied mass transfer and erosion at bends with annular flow through an 180^{o} bend with up-flow. He employed an electrochemical technique and determined the spatial variation of mass transfer. His results showed a strong increase on the outside of the bend just beyond the line of sight position. The mass transfer remained high for the rest of the bend. He concluded that the level of enhancement is a strong function of the gas velocity but did not show much dependence on liquid flow rate. From hydrodynamic studies of annular flow, Usui (1992) noted that the behaviour of the liquid film was greatly affected by the secondary flows caused by the centrifugal forces. This result was confirmed by Chakrabati (1976) in a horizontal 180° bend, Anderson and Hills (1974) in an inverted U, Kooijman and Lacey (1968) and Maddock *et al* (1974) in 60^{o} to 90^{o} bends at the top of a vertical pipe.

Sakamoto *et al*. (2004) carried out experimental work in a horizontal 180^{o} bend using air–water as the working fluid. The diameter and radius of curvature of the bend are 24 and 135 mm, respectively. They employed the conductance type void probe to measure the liquid film thickness and an L-shaped stainless steel sampling tube to measure the local droplet flow rate. They reported the distributions of annular liquid film thickness and the local drop flow rate in the gas core in a straight pipe and at the end of three U-bends at horizontal to horizontal (upward), vertical upward, 45^{o} upward to the horizontal. They claimed that the local flow rate of droplets in the gas core in horizontal pipe flow reaches a minimum near the lower wall of the pipe and a maximum near the upper wall.

Recently, Abdulkadir *et al*. (2012) carried out an experimental investigation on the behaviour of film fraction in a vertical 180^{o} bend using air and water as the model fluids. The diameter and radius of curvature of the bend are 127 and 381 mm, respectively. They carried out measurements of cross-sectional film fraction using conductance ring probes placed at 17 pipe diameters upstream of the bend, 45^{o}, 90^{o} and 135^{o} into the bends and 21 pipe diameters downstream of the bend. The probe was placed 17 D upstream as a compromise between being a well developed flow as far from the mixer as possible and not too close to the start of the bend. The same applies to the 21 D on the outlet. The choice of the measurement locations is justified by the conclusions drawn by Golan and Stenning (1969). They reported that the effect of the bend on phase distribution disappeared by 10 D downstream of the end of the bend for the inverted U-bend case. Abdulkadir *et al.* (2012) concluded that the average film fraction is higher in straight pipes than in bends. And that the condition for which the liquid goes to the outside or inside of the bend can be identified based on a modified form of Froude number, a proposal first made by Oshinowo and Charles (1974). It is worth

mentioning that the averaging effect of the conductance rings can result in differences in the time-varying data, as some details of the asymmetric nature of the liquid film thickness profiles can be affected. In addition, the precise knowledge of the liquid film thickness is complicated by the fact that in many flows of practical interest, such as annular or churn flows, the interface of the film is disturbed by complex waves. Consequently, a probe designed to measure the instantaneous liquid film thickness must accurately measure localized, small-amplitude, high-speed disturbances. These cannot be accurately achieved using the conductance ring probes.

A critical review of the literature, concerning liquid film thickness in bends has revealed that the present state of understanding of liquid film thickness distribution in return bends is limited to two-phase gas–liquid flow in small diameter pipes with air–water as the model fluids. On the matter of large diameter pipes, the only data that was reported is by Abdulkadir *et al*. (2012). In their work, it was the cross-sectional film fraction but not liquid film thickness around the bend being measured. However, obtaining an estimation of the liquid film thickness from the conductance ring probe will lead to an oversimplification of the results. This is because using the film fraction results to obtain liquid film thickness will be based on the assumption of an ideal annular flow in which the liquid flows as a smooth thin film on the pipe wall with the gas in the centre. However, in practice the liquid film is not smooth but covered by a complex system of waves. These waves according to Hewitt and Whalley (1989) and Azzopardi and Whalley (1980) are very important as the sources of the droplets that are entrained in the gas core. Azzopardi *et al*. (1983) reported that the waves in large diameter pipes are circumferentially localised instead of being coherent around the circumference as observed by Hewitt and Lovegrove (1969) for smaller pipes.

It is against these backgrounds that the present work will investigate the behaviour of liquid film thickness distribution in a bend with pipe diameter and bend radius of 127 mm and 381 mm, respectively. The work focuses on churn and annular flows.

2. Experimental apparatus

2.1 Experimental rig and test procedure

The facility used in the present study has been previously reported by Abdulkadir *et al.* (2012) where more details can be found. A brief description of the rig is presented here for the convenience of readers. A schematic diagram of the experimental facility is shown in Figure 1.

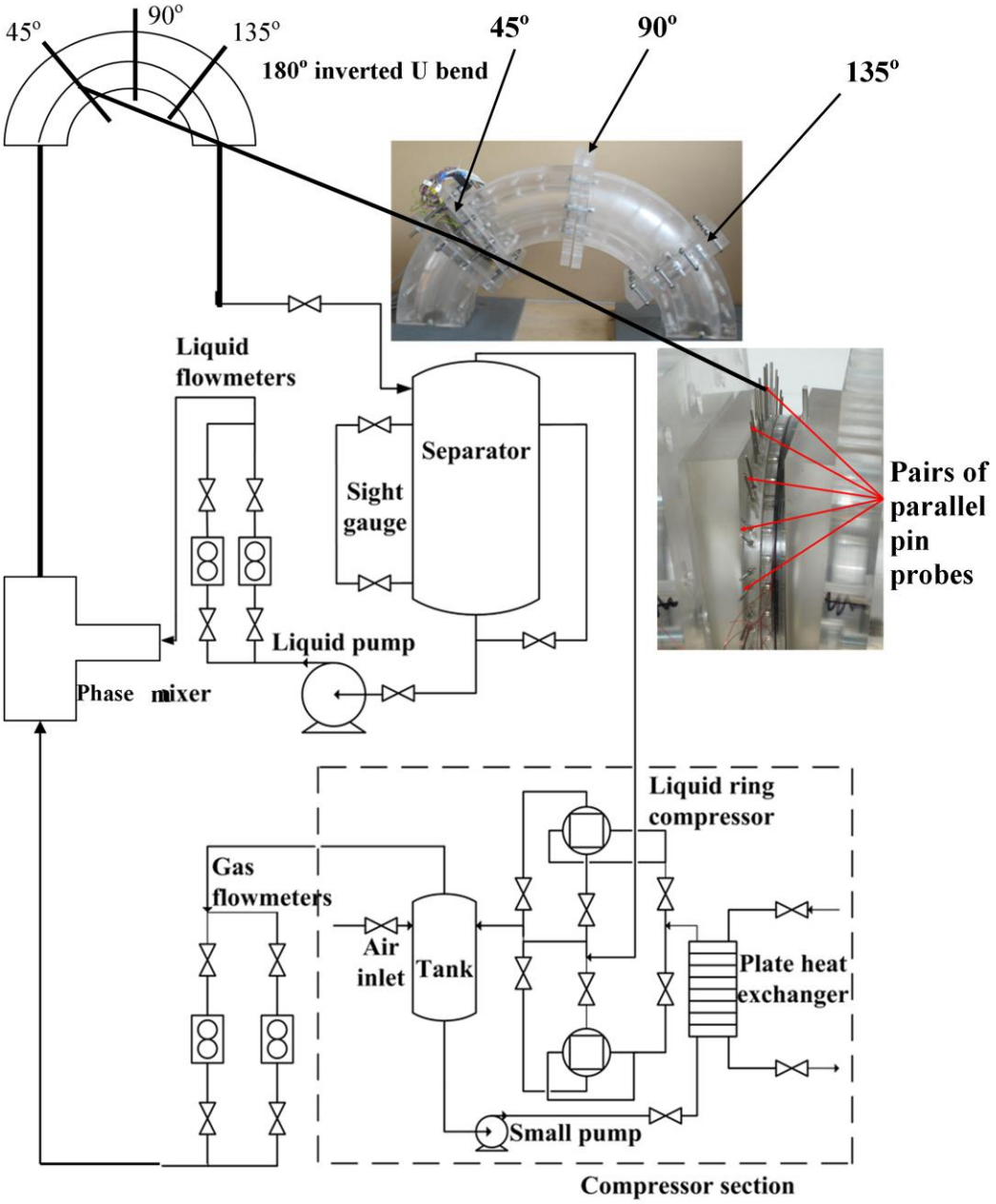

Figure 1: Schematic diagram of the experimental facility

The water stored in the bottom of the separator was pumped to a gas–liquid mixer before it entered the riser, flowed into the bend, went down the downcomer and returned to the separator. The separator is a cylindrical stainless steel vessel of 1 m in diameter and 4 m high filled with 1,600 litres of water. Air used as the gas phase was driven to the gas–liquid mixer by two liquid-ring-pump compressors powered by two 55 kW motors. The gas flow rates were regulated by varying the speed of the compressor motors (up to 1500 rpm) together with

the valves just below the gas flow meters. Before the start of the experiments, the flow loop was pressurised to 2 barg using compressed main air.

Downstream of the mixer, the two-phase mixture travels for 11m along a 127 mm internal diameter vertical riser in which annular or churn flow is established. The test bend with the same internal diameter was mounted on top of the riser. The 180^{o} return bend has a radius of curvature of 381 mm (R/D = 3) and consist of four modular blocks and one instrumentation section containing all the measuring sensors (parallel-ring probes, parallel-wire probes and flush-mounted pin probes). This modular construction enables the measuring section to be inserted every 45^{o} along the bend as shown in Figure 1. Beyond the bend, the air–water flow mixture travels a further 9.6 m vertically downwards in a downcomer and 1.5 m horizontally to the separator where the gas and the liquid are separated and directed back to the compressors and the pump respectively, to create a double closed loop. Care has been taken to ensure that there are no discontinuities of diameter at each joint (Abdulkadir *et al*. (2012)).

In all of these experiments, the temperature of the air and mains tap water was 25^{o} C. The liquid and gas superficial velocities employed were in the ranges from 0.02 to 0.2 m/s and 3.5 to 16.1 m/s, respectively. The experiments were carried out at a pressure of 2 barg.

2.2 Instrumentation

2.2.1 Liquid film thickness measurement

For gas–liquid annular flows in which the liquid is electrically conducting, the conductance measurements are the most widely used technique to measure the liquid film thickness. The technique is based upon measurements of the electrical conductance between two electrodes in contact with the liquid film. Different types of electrodes such as needle probes, parallel

wire probes and flush mounted pin probes have been reported by researchers over the last decades, e.g., Koskie *et al.* (1989), Fossa (1998), Conte and Azzopardi (2003), Belt (2006) and Geraci *et al.* (2007).

The types of probe employed in this study were chosen on the basis of the range of their operability. The liquid film in horizontal annular flow was observed to be asymmetrical with a thick pool at the bottom and a thin liquid film at the top. Liquid film thickness measurements were carried out using a conductance technique, which employed either flush mounted or parallel wire probes. The first type was used for the almost entire section of the pipe while the second type, suitable for higher liquid film thickness, was used only for the bottom section of the bend.

(a) A parallel wire arrangement

Wire probes were originally used by Miya (1970), Miya *et al.* (1971) and Tatterson (1975). According to Brown *et al*. (1978) these probes give a linear response versus liquid film thickness and allow more localised measurements of thicker films to be carried out. Possible objections come from the perturbation which may be induced in the flowing film by the wires and from modifications to the shape of the liquid surface due to the wetting of the wires by liquid. However, in a static film the meniscus which can be observed around thin platinum wires is very small if compared with the liquid film thickness to be measured. According to Brown *et al*. (1978), a more significant disturbance may occur when the probe has to work in a wavy film. When the liquid height decreases, a thin liquid layer sticks to the probe which might indicate a liquid level higher than the actual level, thus introducing a certain amount of lag in the dynamic response of the probe. This phenomenon has been experimentally investigated by Pearlman (1963) who reports these errors to be negligible and that the response of the probe is almost instantaneous. Finally, Brown *et al*. (1978) advised that the

disturbances in the flow caused by stationary wires can be minimised by the use of very thin wires.

In this work, the parallel-wire probes used to measure liquid film thickness at the bottom of the bend are the same type employed by Rea and Azzopardi (2001), Conte (2000), Conte and Azzopardi (2003) and Geraci *et al*. (2007). The parallel wires shown in Figure 2 may also be referred to as a harp arrangement. In this methodology, five pairs of stainless steel wires are stretched along chords of the pipe cross-section and the resistance between pairs measured. According to Miya *et al*. (1971), Brown *et al*. (1978), Koskie *et al*. (1989) and Conte and Azzopardi (2003), the electrodes are two parallel thin wires stretched across a channel or along chords of the pipe or protrude from the wall supported only at one end.

The dimensions of the parallel-wire probe used in this work are shown in Figure 2. The spacing between the two wires of each pair is of 5 mm and the distance between pair is 20 mm, with the central pair placed symmetrically about a vertical diameter. Thin wires based on the recommendations of Pearlman (1963) and Brown *et al*. (1978) were used as the wire probes. The wires have a diameter of 0.33 mm and are stretched across an acrylic resin ring of 25 mm thickness. To ensure proper tension of each wire, plastic screws are inserted in a threaded hole at each end to keep the wires taught. Particular care had to be taken to avoid the wires snapping on the sides of the metallic screw when they were fitted. Because the flow patterns investigated in this study were either annular or churn, precaution had to be taken to eliminate the route for current at the top of the main pipe, across the thin film. The top 15 mm of the wires were insulated with a synthetic waterproof coating to prevent errors being caused by the liquid film at the top of the bend. As the liquid height varies, the surface of active electrode increases and so the resistance decreases because of the larger area of passage for the electric current. The output depends on the geometrical dimensions and on the

conductivity of the medium (liquid). The liquid height (liquid film thickness)/output relationship is obtained by calibration. The response of this system is fairly linear and may be successfully used for thick films. The measurement accuracy of the wire probes according to Brown *et al*. (1978) is within 10 % error. However, for thin films according Conte and Azzopardi (2003), it is a less reliable method because of its intrusive nature, i.e., the formation of a meniscus due to surface tension effects. Also, the local character of measurement depends on the distance between the wires.

The electronic circuit to apply voltage and filtering is the same as used by Rea and Azzopardi (2001), Conte (2000) and Conte and Azzopardi (2003). An a.c carrier voltage of 10 kHz frequency was applied across each pair of electrodes. In this frequency range, measures are strictly reproducible and stable. For details of the electronic circuits and calibration procedure, the reader is referred to Rea and Azzopardi (2001).

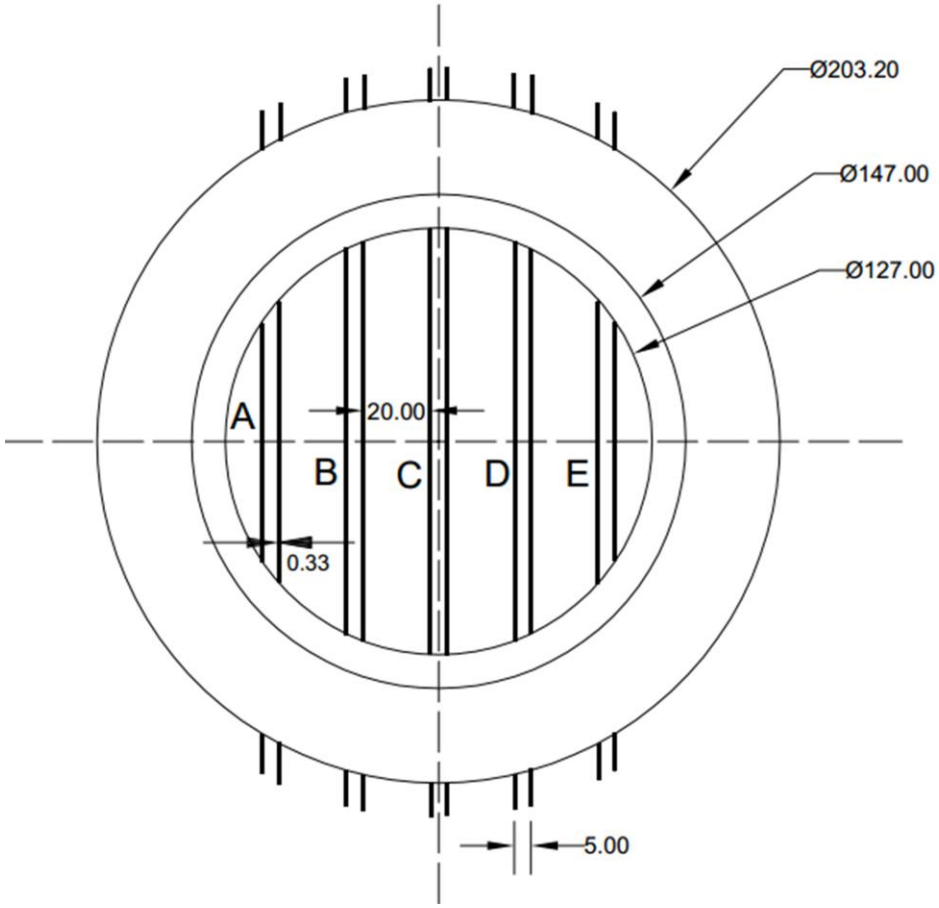

Figure 2: Sketch of the test section for liquid film thickness at the bottom of pipe. Measurements are in mm.

(b) Flush mounted pin probes

This method is used for very thin liquid films, typically up to 2.5 mm. In this case, each electrode is a pin mounted flush with the pipe surface and coupled to another electrode close to it as shown in Figures 1 and 3. If care is taken in the mounting of probes, the method is virtually non-intrusive. The electric field is very weak away from the pipe surface and has a negligible contribution to the passage of current. The response of the pin probe is initially linear to the thickness of the liquid film (typically up to 2 mm) and then asymptotically flattens to a uniform value to the thicker liquid film. This phenomenon is called probe "saturation". When the probe is saturated, its output signal is not sensitive to the change of liquid film thickness. To enlarge the range of measurement, the diameter and separation of pins needs to be increased. However, the greater the spacing, the more averaged is the result

over space. To obtain an optimum measurement of the liquid film thickness therefore, a balance must be struck between range of operability and local character of the measurement (Abdulkadir (2011)). The measured liquid film thickness is assumed to be the value at the mid-point between the centres of the electrodes.

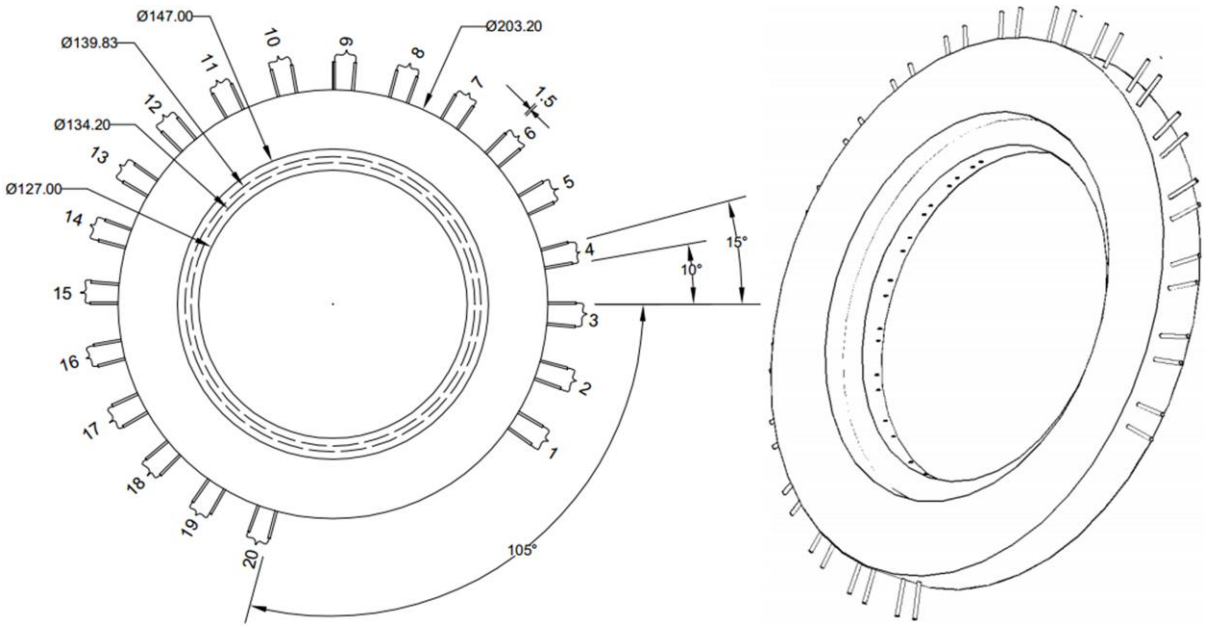

Figure 3: Cross-sectional view of the test section for liquid film thickness measurements at the top of the pipe. Dimensions are in mm.

In the present study, Figure 3 shows the configuration for the test section to locally measure the liquid film thickness on the outside wall without disturbing the flow. The electrodes were spaced by every 10^{o} from each other and 11.84^{o} from the closest wire probe assembly. The probes were made from 1.5 mm diameter welding rods, made of stainless steel to avoid problems of corrosion. The probes were positioned onto the test section by inserting each pair of the electrodes through a cylindrical Perspex rod of 10 mm diameter to ensure accurate location of the probes without causing any damage to the test section. Particular consideration was paid to the different hardness of steel and Perspex so as to avoid jamming of the lathe

and disruption of the test section. This became necessary in order to ensure that the probes were perfectly flush with the inner diameter of the test section. On each side of the test section, 20 pairs of electrodes were located as shown in Figure 3. The sequence is shown on the figure, 1, 2, 3, 4, 5, 6 ... 20. The voltage was applied by an electronic box designed and previously used by Conte (2000) and Conte and Azzopardi (2003); the probes were driven by 10 kHz current. According to Belt (2006), the flow of electrical current from a transmitter in one probe to the neighbour receivers and transmitters (cross–talk) will decrease the spatial resolution of the sensor and increase the measurement errors of the liquid film thickness. To reduce the effect of cross–talking, the 20 pin probes were categorized into 4 groups. The first group classified as A is made up of pins 1, 5, 9, 13 and 17 while pins 2, 6, 10, 14 and 18, as group B. On the other hand, group C is made up of pins 3, 7, 11, 15 and 19 and finally the fourth group classified as D is made up of pins 4, 8, 12, 16, and 20. Moreover all the probes from the four groups were calibrated simultaneously in the same position as they were located in the test section and with the same signal acquisition as has been used during the experiments.

The pin probes were calibrated simultaneously as they were employed during measurements of liquid film thickness around the bend. It was not possible to calculate the response of the instrument. Calibration by simulating the exact geometry of the system was therefore necessary. For this purpose a non-conducting solid rod (PVC) with the same inside and outside diameter as the flow pipe was therefore used for the calibration procedure. Starting from one extremity, the diameter of the rod was reduced progressively by cutting 0.37, 0.62, 1.5, 2, 2.43 and 2.78 mm off the original surface in the radial direction. This was done to produce a static film of liquid on the wall of the test section by filling the annulus between the PVC rod and the pipe wall with a conductive liquid (water). The diameter of the rod was measured with an accuracy of better than $10\,\mu m$ (Zangana (2011)). The rod was centred

correctly at the bottom and the top of the test section using a plastic insert made specifically for that purpose. The calibration was repeated several times and with different rotations as an extra check. The probes were calibrated using water with different conductivities (491, 564 and 600 $\mu S / cm$). The output voltage as a function of liquid film thickness was recorded and as a result the calibration curve for each group of pin probes was obtained.

Tap water, which was used in the experiments, was found to have conductivity between 491 and 600 $\mu S / cm$. If not replaced the water quickly became contaminated and mineral deposits began to show, mostly on the wires. To avoid large variations of conductivity within the same experimental run and to reduce fouling of the electrodes, fresh water was fed continuously to the separator/storage tank and discharged to drain. Calibrations were repeated periodically without cleaning of the electrodes. From the gradient of the signal/liquid film thickness curve and the accuracy of the signal measurement, the uncertainty in liquid film thickness at the top of the pipe is about 11 %. The value for thicker liquid films at the bottom of the bend is much lower.

3. Results and discussion

This work reports the results of a series of studies conducted to investigate the multiphase air–water flow experienced around a 180^o return bend. The parameters which were measured are the local liquid film thickness distribution within the bend, including 45, 90 and 135^o. The ranges of the independent variables, the gas and liquid flow rates, expressed as superficial velocities are given in Table 1. In total, 102 data points were obtained during the test runs for each of the 45, 90, and 135^o bend conditions.

Table 1: The range of variables

u_{gs} (m/s)	u_{ls} (m/s)	Re_{gs}	Re_{ls}
3.5–16.1	0.02–0.2	86413–402,000	2535–25350

3.1 Time averaged cross-sectional liquid film thickness in the 180º bends:

Figure 4 shows a plot of averaged liquid film thickness against bend angle for different liquid and gas superficial velocities. From the figure, the abscissa represents the bend angles considered in this study, 45, 90 and 135º while the averaged liquid film thickness is the ordinate. The averaged liquid film thickness used to plot Figure 4 was obtained by integrating over the cross-sectional area of the local film thickness according to equation 2.

$$\bar{\delta} = \frac{D}{2} - \sqrt{\frac{1}{2\pi}\int_0^{2\pi}\left(\frac{D}{2} - \delta\right)^2 d\theta} \qquad (2)$$

Where $\bar{\delta}$ and δ represent the average and local liquid film thickness, respectively and D is the internal diameter of the pipe.

One interesting observation made in this work is that over the range of liquid flow rates studied, the liquid flow rate has a significant effect on the liquid film thickness distribution in the bend.

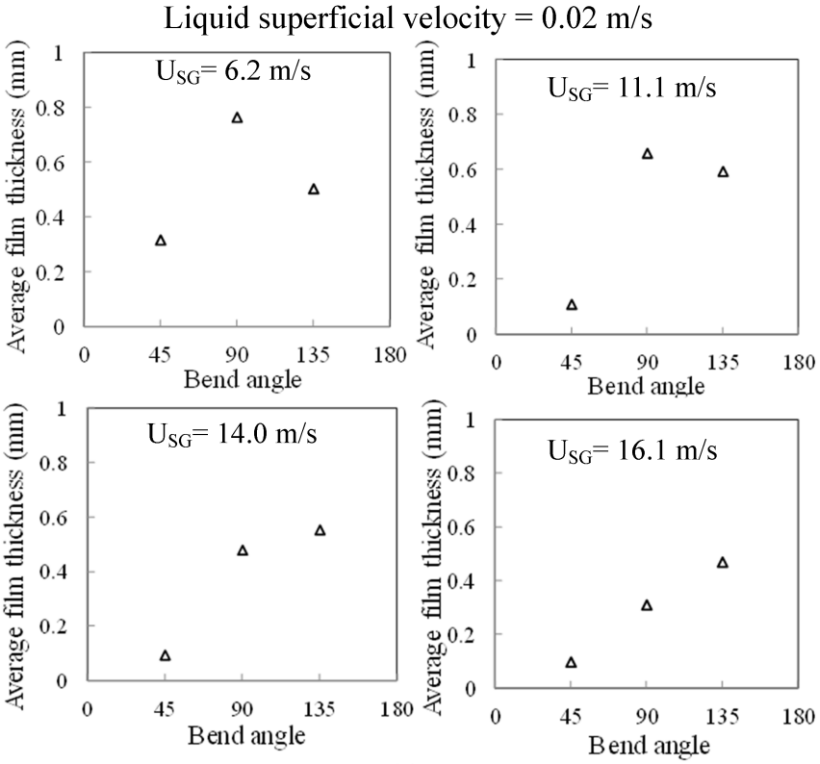
Liquid superficial velocity = 0.02 m/s
U_{SG}= 6.2 m/s
U_{SG}= 11.1 m/s
U_{SG}= 14.0 m/s
U_{SG}= 16.1 m/s
Average film thickness (mm)
Bend angle
0
0.2
0.4
0.6
0.8
1
45
90
135
180

(a)

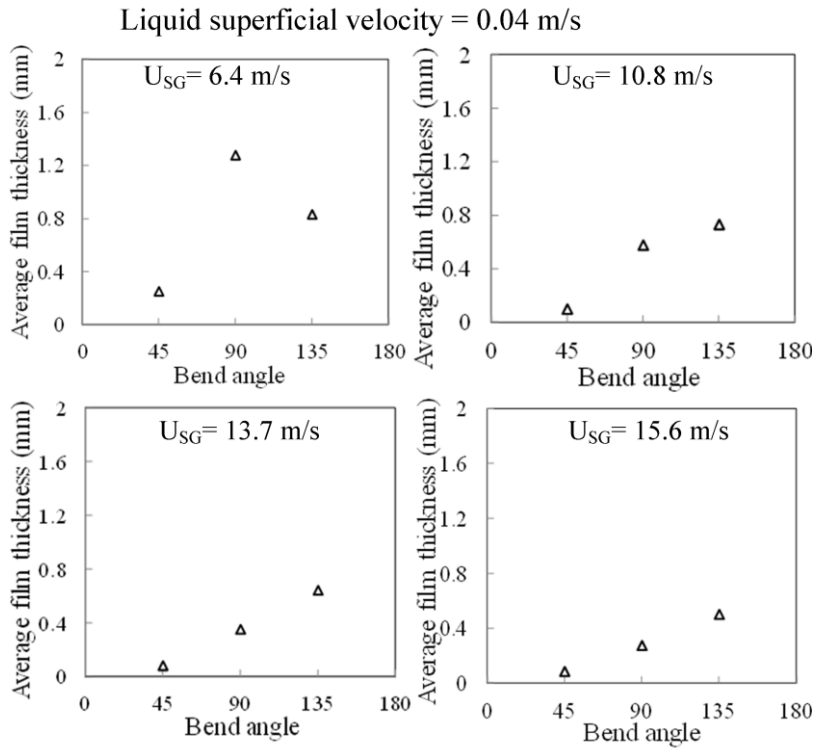
Liquid superficial velocity = 0.04 m/s
U_{SG}= 6.4 m/s
U_{SG}= 10.8 m/s
U_{SG}= 13.7 m/s
U_{SG}= 15.6 m/s
Average film thickness (mm)
Bend angle
0
0.4
0.8
1.2
1.6
2
45
90
135
180

(b)

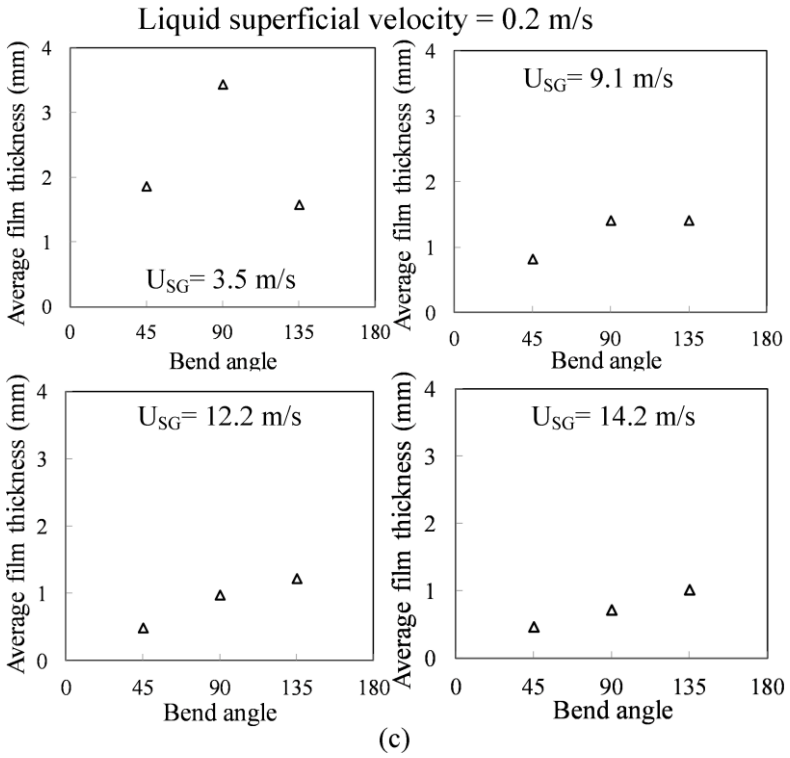

Figure 4: Variation of averaged liquid film thickness with the bend angle at liquid superficial velocity of (a) 0.02 m/s (b) 0.04 m/s and (c) 0.2 m/s

At liquid and gas superficial velocities of 0.02 and 6.2 m/s, the averaged liquid film thickness can be observed to peak at 90^o. This is due to the fact that at this location the effect of gravity is more pronounced and as such drains the liquid to the bottom of the pipe. There is a gradual shift in the location of the maximum average liquid film thickness in the bend, from 90^o to the 135^o bend position as the gas superficial velocity is increased to 14.0 m/s. This is as a consequence of shear forces overcoming gravity and as a result more droplets are deposited at the walls (45 and 135^o bends) supplied with liquid. The end result is that the liquid film at these locations becomes thick. However, because there are more droplets deposited at the 135^o bend, the liquid film is thickest here. At 16.1 m/s gas superficial velocity, there is a linear relationship between the average liquid film thickness and the bend angle. Though, more experimental data are required to substantiate this argument. The entrainment/deposition theory also received some support from the experiments of Laurinat

et al. (1985) using two horizontal pipes with internal diameters of 95.3 mm and 25.4 mm using air–water as the model fluids. They concluded that for the large diameter pipe, entrainment/deposition is the mechanism that maintains the liquid film at the top of the pipe. In addition, they observed waves only at the bottom of the pipe. On the other hand, for the smaller pipe, they concluded that the entrainment/deposition is a dominant factor only for liquid superficial velocities lower than 0.015 m/s.

When the liquid superficial velocity is doubled to 0.04 m/s, and at gas superficial velocity of 6.4 m/s, the same trend that was observed for liquid and gas superficial velocities of 0.02 and 6.2 m/s, respectively is also seen here. Again, the averaged liquid film thickness is observed to peak at 90^{o}. Interestingly, the linear relationship between the average liquid film thickness and the bend angle took place much sooner than that at the lowest liquid superficial velocity. This is because at higher liquid flow rates, the entrainment phenomenon is stronger thereby provoking thickening of the film at the 45 and 135^{o} bends positions.

At liquid superficial velocity of 0.2 m/s and gas superficial velocity of 3.5 m/s, the averaged liquid film thickness can be seen to peak at 90^{o} as indeed observed for the other liquid superficial velocities considered. As the gas superficial velocity is increased further, there is a gradual shift in the position of the film in the bend. At gas superficial velocity of 14.2 m/s, the relationship between the average liquid film thickness and the bend angle is linear.

3.2 Circumferential liquid film thickness variation in the bend:

The variations of the liquid film thickness with four liquid flow rates (0.02, 0.04, 0.08 and 0.1 m/s) are shown in Figure 5. The shape of the profiles varies with the liquid and gas superficial velocities. Here, the polar plots show that at 0.02 m/s and 0.04 m/s liquid superficial velocities and gas superficial velocities of 6.2 m/s and 6.4 m/s, the liquid film distribution is less symmetrical for the three bend angles. But at higher liquid superficial

velocities, the liquid film becomes much thicker at the bottom and is significantly asymmetrical. The plots at liquid superficial velocities of 0.08 m/s and 0.1 m/s show that the profile of the liquid film thickness changes significantly when the bend angle is increased from 45^{o} to 135^{o}. At the 45^{o} and 90^{o} bend positions, the liquid film is thick at the inside of the bend. The thick films become a source of new droplets and at the inside of the 135^{o} bend location; the liquid film is thinner than at the 45^{o} and 90^{o} bend designations. At the inside of the 90^{o} bend position, the liquid film is thicker than that at the 135^{o} but less than that at the 45^{o} bend. This may be due to the deposited droplets falling down owing to gravity drainage as a liquid film at the inside of the 135^{o} bend position. Though, a thickening of the liquid film outside the three bends is also visible, most especially at the 90^{o} and 135^{o} positions. Because the ratio of average liquid film thickness to pipe diameter is very small, the variation of liquid film thickness cannot be seen clearly. It is in view of this development that subsequent results will be displayed in Cartesian coordinates. Figure 6 shows the variation of the time averaged liquid film thickness that occurs in the bend. Here, the abscissa is the circumferential angular position of the probes and the 90 and 270^{o} are the top and bottom of the pipe. 0 and 180^{o} represents the side of the bend.

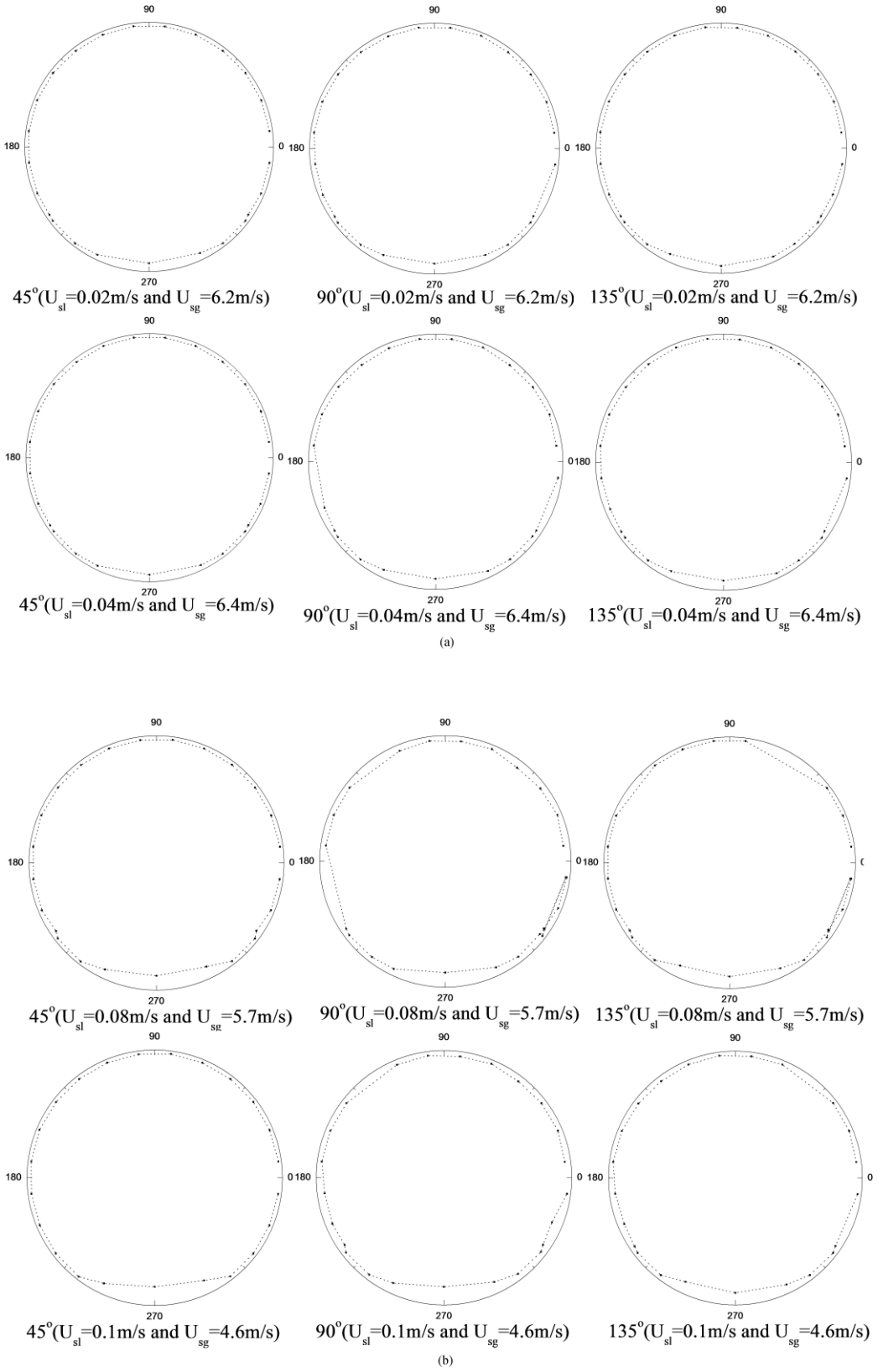

Figure 5: Polar plots of average liquid film thickness in the bend at (a) liquid superficial velocities of 0.02 m/s and 0.04 m/s and (b) liquid superficial velocities of 0.08 m/s and 0.1 m/s. Some points were omitted as shown in some plots based on the fact that they became saturated, most especially at higher liquid flow rates. The pin probes have excellent spatial resolution and thickness resolution for measurements of the order of ≤ 2.5 mm, but became saturated (suffer loss of resolution for thicker films).

3.3 Spatial variations of the average liquid film thickness in the bend:

The average liquid film thickness profiles are presented in Figure 6 that were measured for the 45, 90 and 135^{o} bends. The data collected can be used to understand the variation of liquid film thickness distribution with gas and liquid superficial velocities. Comparison of these profiles shows that the general form of these is greatly influenced by both the gas and liquid superficial velocities. The liquid film thickness inside the bend decreases with increasing gas superficial velocity as the increased interfacial shear produces liquid entrainment in the gas core. In spite of this decrease there are fewer tendencies for film breakdown (when liquid film thickness equals zero) to occur at higher gas rates except at the 45^{o} bend. The same tendency, according to Hills (1973), has been observed for straight pipe horizontal flow with low liquid rates where at higher gas rates stratified flow gives way to annular flow.

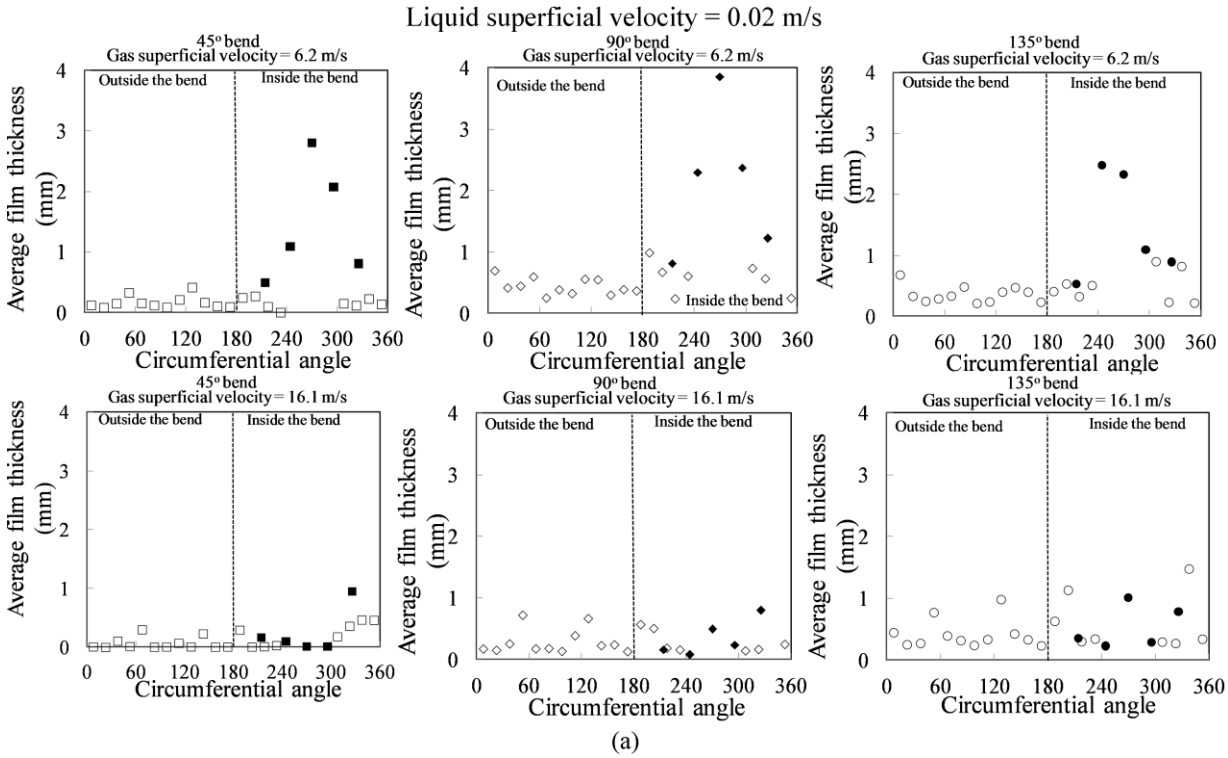

(a)

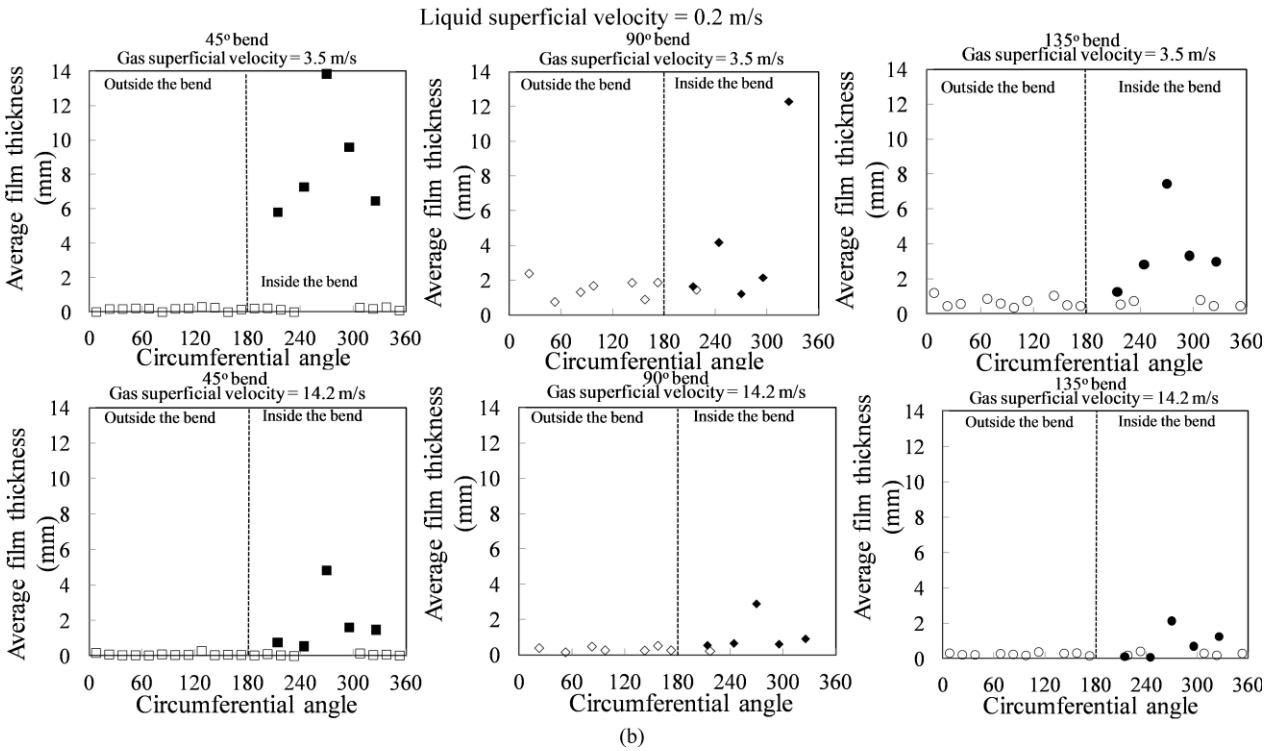

Figure 6: Spatial liquid film thickness distribution at liquid superficial velocity of (a) 0.02 m/s and (b) 0.2 m/s. Closed symbols─wire probes; open symbols─pin probes.

At liquid superficial velocity of 0.02 m/s, the liquid film thickness inside the bend decreases with an increase in gas superficial velocity as shown in Figure 6 (a). In contrast, for the outside of the bend, the liquid film thickness increases and then remains almost constant with an increase in gas superficial velocity. Though, the liquid films are wavy. The decrease in liquid film thickness on the inside of the bend can be attributed to the high interfacial shear stress, bringing about an increase in liquid entrainment in the gas core. The increase on the other hand for the outside of the bend is a result of an increase in droplet deposition outside the bend. This is in agreement with the observations reported by Flores *et al.* (1995). Flores *et al.* (1995) confirmed that a secondary flow exists in horizontal annular flow using a twin axial vorticity meter. They concluded that at low gas velocity the major factor which transports liquid into the upper part of the tube causing the transition from stratified to annular flow is the circumferential secondary flow in the gas core. That at higher gas velocities, the deposition of entrained liquid is a significant factor in transporting liquid to the

top of the tube. In addition, the observations made here supports the arguments presented in Figure 4. At 16.1 m/s gas superficial velocity also, the location of the maximum and minimum liquid film thickness both inside and outside the bend shifts to the 135^{o} and 45^{o} bends, respectively. Though, the change in the magnitude of the liquid film thickness outside the bend is insignificant with an increase in gas superficial velocity.

For 0.2 m/s liquid superficial velocity, the maximum liquid film thicknesses for the inside and outside of the bend are found at 45 and 90^{o}, respectively, as shown in Figure 6b. For the 45^{o} bend, because liquid flow rate is high, the centrifugal force therefore has a greater influence and acts on it like a cyclone: throwing the liquid to the outside of the bend. Gravity on the other hand, drains the liquid to the bottom of the pipe. In addition, some of the liquid that is meant to move up to the 90^{o} bend due to its lower momentum and curvature of the bend return back (back flow) to the 45^{o} bend. These two scenarios could be the explanation for why the observed liquid film at the bottom of the 45^{o} bend is thicker than the other locations, 90 and 135^{o} bend locations. Some of the liquid at the bottom and top of the 90^{o} bend due to the action of gravity and shape of the curvature of the bend, drain down to the bottom of the 135^{o} bend and accumulate there. Also the droplets that impinged on the wall also deposit at the 135^{o} bend. This could be the reason why there is a thick film at the 135^{o} bend but less than those found at the 45^{o} and 90^{o} bends. This claim is supported by analyzing the images taken by a high speed video camera. For the outside of the bend scenario, the liquid film is thickest at the 90^{o}, followed by the 135^{o} and thinnest at the 45^{o} bend. The film is wavy. This is an indication that more liquid is drained from the top of the 45^{o} bend. As a consequence of this drainage, the liquid film at the outside of the 45^{o} bend thins out and become more uniformly distributed around it. The uniformity of the liquid film could be due to a balance of circumferential drag, shear and gravity forces. Another possible explanation could be that the pin probes that are meant to cope with thin liquid films could not see the

expected thick films outside the 45^o bend. At gas superficial velocity of 14.2 m/s, as expected the location of the liquid film inside the bends in increasing order are 135^o, 90^o and 45^o, respectively. This therefore suggest that the reverse flow of liquid that was observed for the 90^o bend at gas superficial velocity of 3.5 m/s is not seen here: most of the liquid is able to climb up into the bend and accumulate there. For the outside of the bend, most of the liquid at higher gas flow rate are being drained to the bottom of the bend and as a consequence the liquid thins out in the 3 bends.

It can be concluded that contrary to the observations reported by Hills (1973) and Anderson and Hills (1974), with regards to liquid film distribution at higher liquid flow rates and lower gas flow rates, the liquid film thickness on the inside of the bend is indeed thicker than on the outside. Three reasonable explanations suggest themselves: (1) Anderson and Hills (1974) used a bend with a curvature ratio 4 times that of the present study and the implication is more liquid film is drained from the top to the bottom of the bend. (2) The ratio of surface tension to pipe diameter in this study is small, experiments therefore suggest that the effect of gravity has overcome the circumferential drag and as a result the liquid film drains to the bottom of the bend. (3) The pin probes could not cope with thicker films greater than 2.5 mm and became saturated as a consequence suggests a thinning of the liquid film. As the gas superficial velocity is increased further, the film at the outside of the bend drains out almost completely.

3.4 Comparison between Experiments and Previous Computational Fluid Dynamics (CFD) Studies Based on Spatial Liquid Film Thickness Variation in the Bend:

Some disagreements were observed in the data reported by Hills (1973), Anderson and Hills (1974) and the present experimental study with regards to liquid film distribution in the bend. The reason can be argued by the fact that in the present study the pipe diameter and radius of curvature are different. In order to actually find out if the present data is consistent, there was

a need to compare experimental data against similar pipe configuration. Hitherto, no such experimental data was found in the literature. The aim of this section therefore is to compare and verify whether CFD calculations are consistent with the experimental observations discussed earlier. The CFD calculations were carried out by Tkaczyk (2011) using similar pipe configuration and dimensions, fluid properties and operating conditions to the experiment. He modelled the gas–liquid flow as a continuum gas field, continuum liquid film and as liquid droplets of varying diameters. The dynamics of the droplet flow in the gas core and the interaction between them were accounted for. The liquid film was explicitly solved using a modified Volume of Fluid (VOF) method. The droplets were tracked using a Lagrangian technique. The liquid film to droplet and droplets to liquid film interactions were taken into account using sub-models to complement the VOF model. He took into cognizance the fact that in free surface flows, a high velocity gradient at the gas/liquid interface results in high turbulence generation. In order to overcome this shortcoming, he implemented a correction to the VOF model based on the work of Egorov (2004). Full details can be found in Tkaczyk (2011). The model gives a reasonably good prediction of the liquid film thickness in the bend. Figure 7 shows the comparison between the experimental results and those obtained numerically by Tkaczyk (2011).

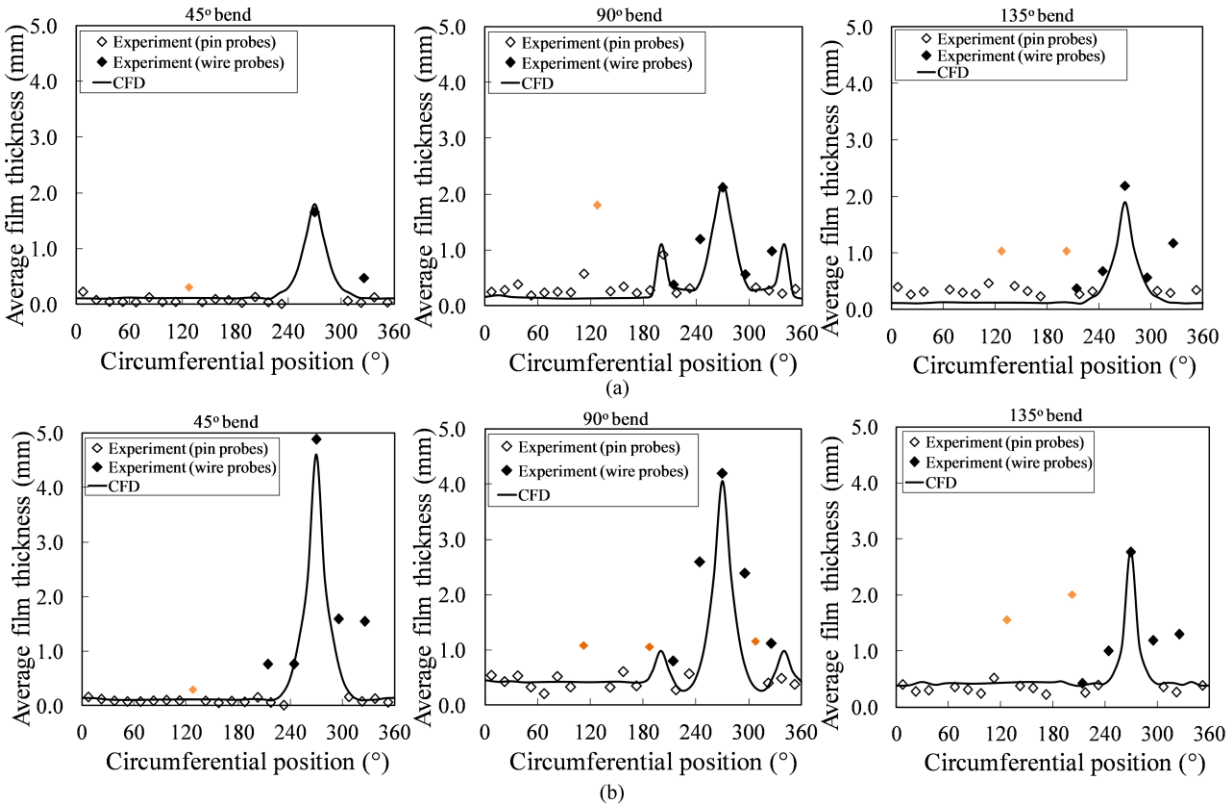

Figure 7: The distribution of liquid film thickness in the bend at (a) liquid and gas superficial velocities of 0.1 and 11.24 m/s, respectively and (b) liquid and gas superficial velocities of 0.2 and 12.5 m/s, respectively. Angles 0–180° represents outside the bend and 181–360°, inside the bend. Closed symbols-wire probes; open symbols-pin probes; grey symbols represents film thickness measurement with less confidence.

At liquid and gas superficial velocity of 0.1 and 11.24 m/s, respectively the model under predicts the film thickness outside the 90 and 135° bends. It also under predicts the maximum film thickness inside $(\theta = 270^{o})$ the 135° bend with an error of 13.2 %. It is interesting to note that the model is able to predict the maximum film thickness inside the 45 and 90° bends. It is also able to predict the film thickness outside the 45° bend. Though, the error is 8.3 %. Another interesting observation made here is that the double peak found on the film thickness which Adechy and Issa (2004) made an effort to replicate without success is correctly predicted. Adechy and Issa (2004) used a Lagrangian/Eulerian approach to simulate annular flow in a T-junction. They represented the liquid film as a thin film model based on the assumption that the liquid film is thin and behaves like a boundary layer, so that the

dominant derivatives are in the direction normal to the flow. Although, the first and second peaks separated by the maximum film thickness are shown to occur respectively at a position 200^o and 340^o. The former occurring at 2.5^o less than that found experimentally whiles the latter 14.2^o more.

At liquid superficial velocity of 0.2 m/s and gas superficial velocity of 12.5 m/s, the model is able to predict the maximum film thickness inside and outside the 135^o bend except for some few points outside. The model under predicts the maximum film thickness inside the 45 and 90^o bends. The percentage error of the former is 5.7 whilst for the latter, 3.3. However, it is able to predict the film thickness outside the 45^o bend well.

It can be concluded therefore that the comparison between CFD results and experiment is very good and that the present experimental data have been successfully used to validate models for the prediction of spatial film thickness variation in the bend.

4. Conclusions:

A comprehensive set of measurements has been taken to study the effect of liquid film thickness distribution in a bend of 127 mm internal diameter and bend radius of 381 mm at various gas and liquid flow rates. The liquid film thickness distribution in the bend has been measured with pin and wire probes. With the former for measuring thin films ≤ 2.5 mm outside the bend while the latter for thick liquid films ≥ 2.5 mm inside the bend. These measurements have been supplemented by visual observation.

1) For liquid and gas superficial velocities of 0.02 m/s and 6.2 m/s, respectively, the averaged liquid film thickness was observed to peak at 90^o. As the gas superficial velocity is gradually increased to 14.0 m/s, the triangular relationship begins to diminish and tends towards linear. At the higher liquid superficial velocities, this change took place at the lower gas superficial velocities.

2) The results of polar plots of average liquid film thickness in the bend showed that the distribution of the liquid film is not symmetrical with thicker films on the inside of the bend due to the action of gravity.
3) Deposition of entrained droplets, which has a higher momentum than the gas which carries them, keeps the film on the outside of the bend supplied with the liquid. This is consistent with the observations reported by Flores *et al.* (1995). This will be of vital importance in applications where it is desirable to maintain a liquid film on the pipe wall.
4) At higher liquid flow rates, although the liquid film thickness is always relatively high on the inside of the bend due both to the lower interfacial shear stress and gravity drainage of the liquid film to the bottom of the pipe. The liquid film thins out in the three bends location.
5) The comparison between CFD results reported in literature and experiment showed a good agreement. The double peak found on the liquid film thickness which Adechy and Issa (2004) failed to replicate is correctly predicted by Tkaczyk (2011).

5. Acknowledgements

M. Abdulkadir would like to express sincere appreciation to the Nigerian government through the Petroleum Technology Development Fund (PTDF) for providing the funding for his doctoral studies.

D. Zhao was funded by EPSRC under grant EP/ F016050/ 1 and A. Azzi held a visiting Research fellowship under the same grant.

The Author(s) wish to express their sincere gratitude for this support.

6. References:

Abdulkadir, M., 2011. Experimental and computational fluid dynamics (CFD) studies of gas-liquid flow in bends. PhD Thesis, University of Nottingham, United Kingdom.

Abdulkadir, M., Zhao, D., Azzi, A., Lowndes, I.S., and Azzopardi, B.J, 2012. Two-phase air–water flow through a large diameter vertical 180^o return bend. Chemical Engineering Science 79, 138-152.

Adechy, D and Issa, R. I., 2004. Modelling of annular flow through pipes and T-junctions. Computers and Fluids 33, 289-313.

Alves, G. E., 1954. Co-current liquid–gas flow in a pipeline contactor. Chemical Engineering Progress 50, No. 9:449.

Anderson, G.H., and Hills, P. D., 1974. Two-phase annular flow in tube bends. Symposium on Multiphase flow Systems, University of Strathclyde, Glasgow, Paper J1, Published as Institution of Chemical Engineers Symposium, Series No. 38.

Azzopardi, B. J., Taylor, S., and Gibbons, D.B., 1983. Annular two phase flow in large diameter pipes. Proceedings of the International Conference on the Physical Modelling of Multiphase Flow, Coventry, 256-267.

Azzopardi, B. J., and Whalley, P. B., 1980. Artificial waves in annular two phase flow. ASME Winter Annual Meeting, Chicago, published in Basic Mechanics in Two Phase Flow and Heat Transfer

Balfour, J. D., and Pearce, D.L., 1978. Annular flows in horizontal 180^o bends: measurements of water rate distributions in the film and vapour core. C.E.R.L. Note No. RD/L/N96/78.

Belt, R.J., 2006. On the liquid film in inclined annular flow. PhD thesis, Delft University of Technology, Netherlands.

Brown, R.C., Andreussi, P., and Zanelli, S., 1978. The use of wire probes for the measurement of liquid film thickness in annular gas–liquid flows. The Canadian Journal of Chemical Engineering 56, 754-757.

Chakrabati, P., 1976. Some aspects of annular two-phase flow in a horizontal tube. PhD thesis, Imperial College, London.

Chong, L. Y., Azzopardi, B. J., and Bate, D. J., 2005. Calculation of conditions at which dryout occurs in the serpentine channels of fired reboilers. Chemical Engineering Research and Design 83, 412-422.

Conte, G., 2000. An experimental study for the characterisation of gas/liquid flow splitting at t-junctions. PhD thesis, University of Nottingham, United Kingdom.

Conte, G., and Azzopardi, B.J., 2003. Film thickness variation about a T-junction. International Journal of Multiphase Flow 29, 305-325.

Egorov, Y., 2004. Contact condensation in stratified steam–water flow. EVOL-ECORA-D 07.

Flores, A.G., Crowe, K.E., and Griffith, P., 1995. Gas-phase secondary flow in horizontal, stratified and annular two-phase flow. International Journal of Multiphase flow 21, 207-221.

Fossa, M., 1998. Design and performance of a conductance probe for measuring the liquid fraction in two-phase gas–liquid flows. Flow Measurement and Instrumentation 9, 103-109.

Geraci, G., Azzopardi, B.J, and Van Maanen, H.R.E., 2007. Inclination effects on circumferential film distribution in annular gas/liquid flows. *AIChE* Journal 53, 1144-1150.

Golan, L.P., and Stenning, A.H., 1969. Two-phase vertical flow maps. Proceedings of the Institution of Mechanical Engineers 14.

Hewitt G. F., and Lovegrove, P.C, 1969. Frequency and velocity measurements of disturbance waves in annular two-phase flow. UKAEA Report AERE-R4304.

Hewitt, G. F., and Whalley, P. B., 1989. Vertical annular two phase flow. Multiphase Science and Technology 4, Chapter 2, Hemisphere Publishing, New York.

Hills, P. D., 1973. A study of two-phase (gas–liquid) flow in a tube bend. PhD Thesis, Imperial College, London, United Kingdom.

Hoang, K., and Davis, M.R., 1984. Flow structure and pressure loss for two phase flow in return bends. Journal of Fluids Engineering 106, 30-37.

Koskie, J.E., Mudawar, I., and Tiederman, W.G., 1989. Parallel wire probes for measurement of thick liquid films. International Journal of Multiphase flow 15, 521-530.

Kooijman, J., and Lacey, P.M.C., 1968. Unpublished internal report. Department of Chemical Engineering, University of Exerter.

Laurinat, J.E., Hanratty, T.J., and Jepson, T.W., 1985. Film thickness distribution for gas–liquid annular flow in a horizontal pipe. PhysicoChem. Hydrodynamics 6, 179-195.

Maddok, C., Lacey, P.M.C., and Patrick, M.A., 1974. The structure of two-phase flow in a curved pipe. In: Symposium on Multiphase Flow Systems, Institution of Chemical Engineers Symposium Series, University of Strathclyde, paper J2 38.

Mandhane, J.M., Gregory, G.A., and Aziz, K., 1974. A flow pattern map for gas–liquid flow in horizontal pipes. International Journal of Multiphase Flow 1, 537-553.

Miya, M., 1970. Properties of roll waves. PhD thesis, University of Illinois, Urbana, USA.

Miya, M., Woodmansee, D.E., and Hanratty, T.J., 1971. A model for roll waves in gas–liquid flow. Chemical Engineering Science 26, 1915-1931.

Oshinowo, T., and Charles, M. E., 1974. Vertical two-phase flow- Part 1: Flow pattern correlations. Canadian Journal of Chemical Engineering 52, 25-35.

Pearlman, M.D., 1963. Dynamic calibration of wave probes. Department of Naval architecture and Marine Engineering, MIT, USA.

Poulson, B., 1991. Measuring and modelling mass transfer at bends in annular flow two-phase flow. Chemical Engineering Science 46, 1069-1082.

Rea, S., and Azzopardi, B. J., 2001. The split of horizontal stratified flow at a large diameter T-junction. Transaction of the Institution of Chemical Engineers 79 A, 470-476

Sakamoto, G., Doi, T., Murakami, Y., and Usui, K., 2004. Profiles of liquid film thickness and droplet flow rate in U-bend annular mist flow. 5th International Conference on Multiphase Flow, ICMF 2004, Japan, May 30-June 4.

Smith, A. V., 1971. Transient density measurement in two-phase flows using X-rays. Journal of British Nuclear Society 10, 99-106.

Takemura, T., Roko, K., and Shiraha, M., 1996. Dryout characteristics and flow behaviour of gas–water flow through U-shaped and inverted U-shaped bends. Nuclear Engineering Design 95, 365-373.

Tatterson, D.F., 1975. Rates of atomization and drop size in annular two-phase flow. PhD thesis, University of Illinois, Urbana, USA

Tingkuan, C., Zhihua, Y., and Qian, W., 1986. Two-phase flow and heat transfer in vertical U-shaped tubes (I) Flow pattern transitions in the bend. Journal of Chemical Industry and Engineering (China) 1, 1-12.

Tkaczyk., P., 2011. CFD simulation of annular flows through bends. PhD thesis, University of Nottingham, United Kindom.

Usui, K., 1992. Annular two-phase flow in a C-shaped bend (liquid film flow). Transactions of the Japan Society of Mechanical Engineers 58, 200-205.

Usui, K., Aoki, S., and Inoue, A., 1980. Flow behaviour and pressure drop of two-phase flow through C-shaped bend in a vertical plane-I: Upward flow. Journal of Nuclear Science and Technology 17, 875-887.

Usui, K., Aoki, S., and Inoue, A., 1981. Flow behaviour and pressure drop of two-phase flow through C-shaped bend in a vertical plane-II: Down flow. Journal of Nuclear Science and Technology 18, 179.

Usui, K., Aoki, S., and Inoue, A., 1983. Flow behaviour and phase distributions in two-phase flow around inverted U-bend. Journal of Nuclear Science and Technology 20, 915-928.

Weisman, J., and King, S.Y., 1981. Flow pattern transitions in vertical and upwardly inclined lines. International Journal of Multiphase flow 7, 271-291.

Yu, Q.G., Barrier, D., Cognet, G., 1989. Two-phase flow in horizontal and vertical C-types of bend- Pressure and void fraction distribution. European Two-Phase Flow Group Meeting, Paris.

Zangana, M., 2011. Film behaviour of vertical gas–liquid flow in a large diameter pipe. PhD thesis, University of Nottingham, United Kingdom.

Figure captions:

Figure 1 Schematic diagram of the experimental facility

Figure 2 Sketch of the test section for liquid film thickness at the bottom of pipe

Figure 3 Cross-sectional view of the test-section for liquid film thickness measurement at the top of the pipe

Figure 4 Variation of average liquid film thickness with the bend angle at liquid superficial velocity of (a) 0.02 m/s (b) 0.04 m/s and (c) 0.2 m/s

Figure 5 Polar plots of average liquid film thickness in the bend at (a) liquid superficial velocities of 0.02 m/s and 0.04 m/s and (b) liquid superficial velocities of 0.08 m/s and 0.1 m/s

Figure 6 Spatial liquid film thickness distributions at liquid superficial velocity of (a) 0.02 m/s (b) 0.2 m/s

Figure 7 The distribution of liquid film thickness in the bend at (a) liquid and gas superficial velocities of 0.1 and 11.24 m/s, respectively and (b) liquid and gas superficial velocities of 0.2 and 12.5 m/s, respectively.

Table captions:

Table 1 The range of variables